Reprint from

"PLASMA PHYSICS AND CONTROLLED NUCLEAR FUSION RESEARCH"

VOL.I

INTERNATIONAL ATOMIC ENERGY AGENCY
VIENNA, 1969

EFFECT OF SHEAR AND CONNECTION LENGTH ON DRIFT WAVES AND PLASMA CONFINEMENT *

F. F. CHEN, D. MOSHER † AND K. C. ROGERS ‡
PLASMA PHYSICS LABORATORY, PRINCETON UNIVERSITY,
PRINCETON, N.J., UNITED STATES OF AMERICA

Abstract

EFFECT OF SHEAR AND CONNECTION LENGTH ON DRIFT WAVES AND PLASMA CONFINEMENT. We have investigated separately the effectiveness of shear and of short connection length on drift instabilities in a 0.22 eV thermally-ionized, 3-meter long potassium plasma. These experiments were carried out with T_i/T_e and ρ_i/R in a regime comparable to what would obtain in a fusion reactor. In the density range $n = 10^9 - 10^{11}$ cm^{-3}, we cover the transition from collisionless to collisional excitation of drift waves; ion viscosity is important only at highest densities studied.

By tailoring the radial electric field, it is possible to produce quiescence, turbulence, or single modes. Shear is applied by passing current through a 1-cm diam. hard core along the axis. Both turbulent and coherent drift waves are stabilized by shear of order $\theta \sim 0.05$, in fair agreement with the theory of Krall and Rosenbluth. However, at large shear, small-amplitude coherent oscillations reappear unexpectedly.

At zero shear, $D_\perp$ is 2-3 times the Bohm diffusion coefficient; at maximum shear, $D_\perp$ is decreased a factor of 5-30 to 2-3 times the classical value. At least half of $D_\perp$, however, is not connected with oscillations at all; it is due to the d.c. drifts in weak asymmetric electric fields produced by temperature variations at the end plate. The twisting of the equipotentials into spirals and thus symmetrization of the E fields has been observed in detail experimentally. A finite-Larmor-radius theory for the effect of shear in reducing the radial drift is found to be in agreement with the observed reduction in $D_\perp$.

Short connection length is achieved by internal current loops providing a B_z opposing the main B_z, thus creating stagnation points lying on the axis. In the vicinity of each ring, the plasma is bent around the ring and is stabilized by both minimum-$\bar{B}$ and viscous damping. The rings are spaced 75-180 cm apart, and between rings the field is uniform. Thus, instabilities are restricted to those with short $\lambda_\parallel$. We find that the oscillation level is greatly reduced by current in the rings.

We conclude that 1) radial electric fields affect not only the frequencies but also the excitation thresholds of drift waves; 2) it is easy, with small shear or minimum-$\bar{B}$, to reduce oscillations to a level at which they contribute negligibly to anomalous transport; and 3) the primary loss mechanism is steady convection along asymmetric equipotentials, and large shear can reduce the loss rate by twisting the equipotentials into long spirals.

1. INTRODUCTION AND APPARATUS

Drift waves in an inhomogeneous plasma can be stabilized by a) magnetic or velocity shear and b) minimum-$\bar{B}$ with short connection length between regions of favorable curvature. In this paper we summarize four experiments designed to test separately the effectiveness of each method in suppressing oscillations and decreasing anomalous plasma transport. The experiments were carried out in a thermally ionized potassium plasma (Q machine) in which currents and mass flow along $\underset{\sim}{B}$ were carefully minimized. A diagram of the machine in the shear configuration is shown in Fig. 1. The 326-cm length of the plasma between the hot plates allows waves of small $k_\parallel$ to grow in spite of

* Supported under the auspices of the US Atomic Energy Commission.

† Present address: Los Alamos Scientific Laboratory, Los Alamos, New Mexico.
‡ Permanent address: Stevens Institute of Technology, Hoboken, N.J.

line-tying by the electron sheaths at each end plate [1]. At 4 kG, the ion gyroradius r_L is 0.1 cm, so that there are 5 - 10 gyroradii in a density scale length r_0 in the hard-core configuration; the ratio r_L/r_0 is comparable to that in the present generation of multipoles. By varying the density n , the mean free path can be varied from 100 cm down to less than 1 cm.

In thermionic plasmas the radial electric field E_r is primarily determined by the equation

$$j_T \exp(e\phi/KT) = \frac{1}{4} n v_e \qquad (1)$$

expressing the balance between random electron current striking the end plates and the thermionically emitted current, attenuated by the Coulomb barrier of the sheath. Here j_T is the Richardson current $j_T = AT^2 \exp(-e\phi_w/KT)$, and ϕ is the (negative) potential drop from the end plate surface to the sheath edge. Since n varies with radius, so will ϕ. The resulting E_r causes a plasma rotation which Doppler shifts the electron diamagnetic velocity $\vec{v}_{De} \equiv -(KT/eB)(n'/n)\vec{\theta}$ to zero in the laboratory frame and the ion diamagnetic velocity $\vec{v}_{Di} = -\vec{v}_{De}$ to $2\vec{v}_{Di}$. However, deviations from this "normal" E_r occur when small temperature gradients in the end plates cause large variations in j_T, and when ion-ion collisions allow a nonvanishing mobility across $\vec{B}$. These effects are important in understanding the results which follow.

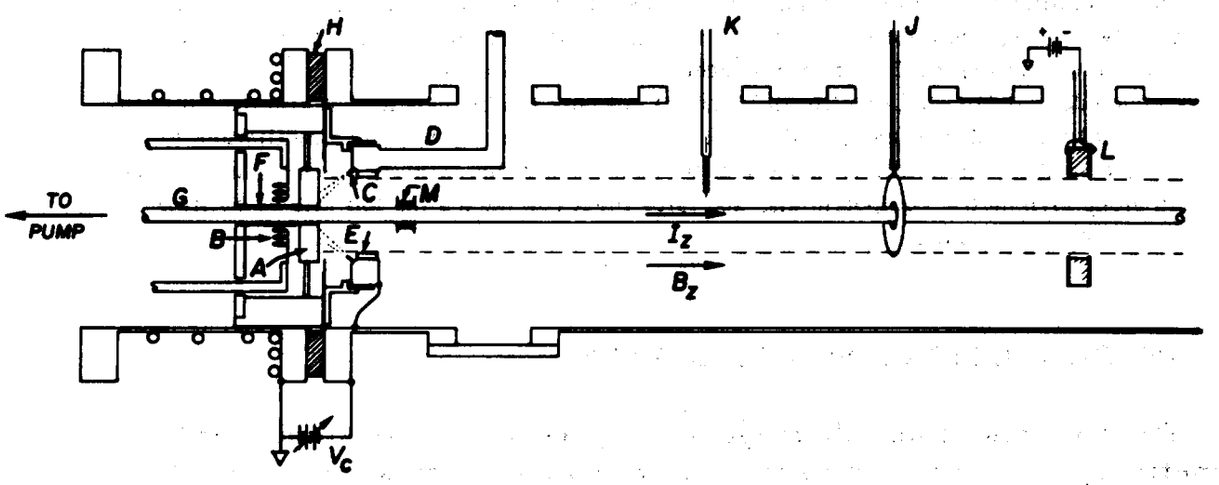

FIG. 1. Schematic diagram showing one end of the hard-core Q machine; the other end is identical and is located 3 metres away. The tungsten hot plate A is heated to 2550°K by electron bombardment from the filament B. Neutral potassium atoms impinging on A are collimated by 16 small pipes C emanating from an annular chamber fed by the heated pipe D. The plasma aperture is defined by the limiter E. The grounded molybdenum tube F prevents fast electrons from entering the plasma. The hard core G is a water-cooled, anodized aluminium tube 1 cm in diameter threaded through 1.3 cm diameter holes in the hot plates and kept straight by 500 kg of tension. The ceramic break H allows the vacuum chamber, including the aperture limiter E, to be biased at a potential V_c relative to the grounded hot plates. The collector J measures the total flux of ions emitted from the hot plate; J is split so as to be removable. K is a typical Langmuir probe. L is a plasma catcher for measuring the radial losses to the outside. The inner limiter M can also be used to measure losses to the inside and to set the plasma potential at the inner boundary. The plasma diameter is 5.08 cm, and all positions are approximately to scale, except that L is normally at the midplane of the machine.

2. ANOMALOUS TRANSPORT BY PLASMA CONVECTION

When the neutral input flux Φ_{in} is kept constant, we have previously reported [2] that the plasma density increases by more than an order of magnitude as the hard-core current I_s is increased to its maximum value of 4 kA d.c. This effect is illustrated in Fig. 2, which shows the increase in n with I_s. The curve n_{osc} is a lower limit on the density expected if losses were due to oscillations alone; this limit is obtained from the oscillation amplitude n_1 and the assumption that n_1 and potential ϕ_1 are 90° out of phase. It is seen that above I_s = 200 A, the density is limited by a shear-dependent loss mechanism not related to oscillations.

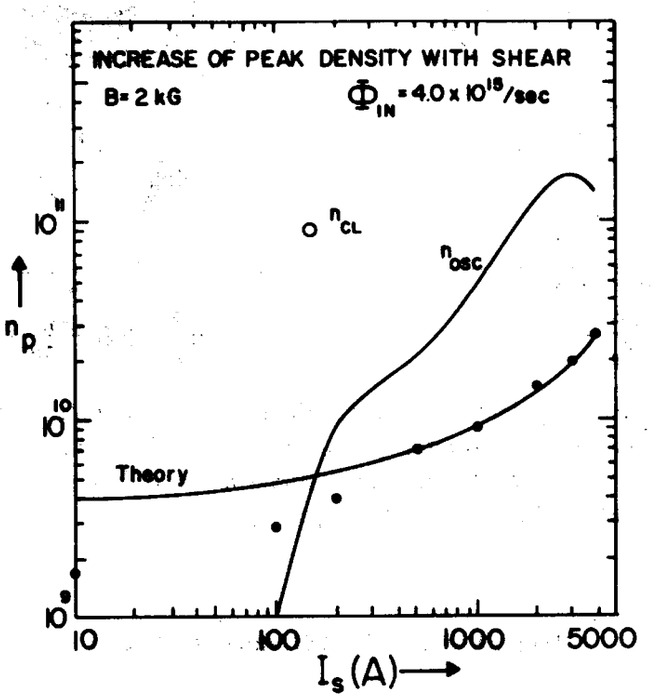

FIG. 2. Increase of peak density n_p with current in the hard core. The point n_{c_1} is the density expected from classical processes alone (resistive diffusion and end-plate recombination).

Such a mechanism is the steady convection of plasma along equipotentials which are not concentric with the plasma. According to Eq. (1), asymmetries in the distribution of plasma potential ϕ can arise from azimuthal gradients in end-plate temperature T and hence in j_T. This effect has been verified by direct pyrometric measurements ($\Delta T \approx \pm 15^{\circ}$ K in our case). When shear is applied, the radially varying rotational transform causes the equipotentials to be twisted into long spirals, as shown in Fig. 3, because potential is approximately constant along a line of force. This has the effect of symmetrizing the drift surfaces, and ions must $\vec{E} \times \vec{B}$ drift a longer distance to change radial position. [Note that electrons are not confined because of the Simon short-circuit effect and need only satisfy Eq. (1).]

The existence of spiral convective cells is revealed by radial scans of probe floating potential, as shown in Fig. 4 for two values of I_s. These patterns are steady and reproducible. The spacing Δr between spiral arms is found to vary as r^3, as expected from theory.

By probing the entire cross section, one can plot the equipotential contours shown in Fig. 5 for two different distances from the hot plate. These observations confirm the existence of spiral convective patterns in the presence of shear. We next compute the increase in confinement time arising from this effect.

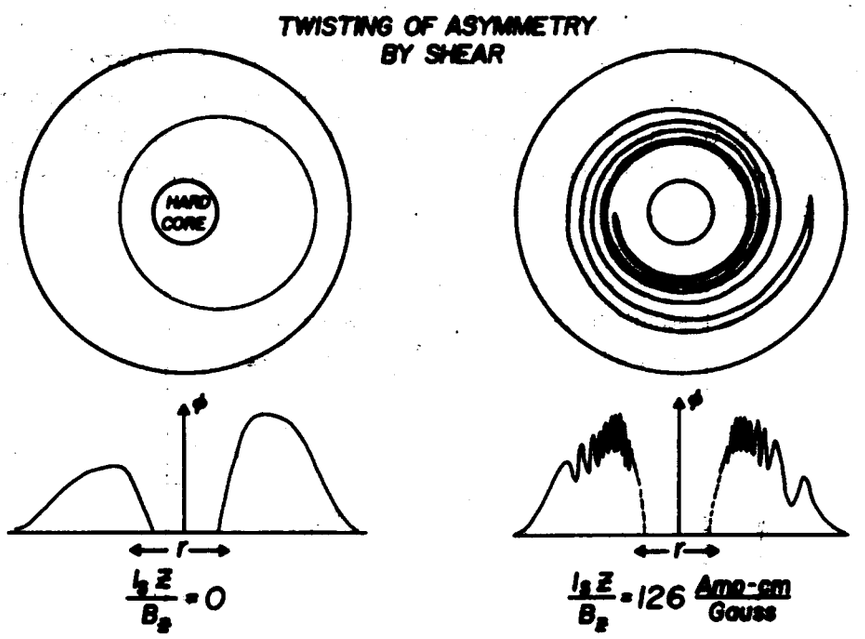

FIG. 3. Schematic of how an equipotential contour with an m = 1 asymmetry can be twisted into a spiral by shear, characterized by the parameter $I_z z/B_z$, where z is the axial separation between the two cross-sections depicted. Radial profiles of plasma potential ϕ are shown below. In double-ended operation, the spirals from each end plate are superimposed.

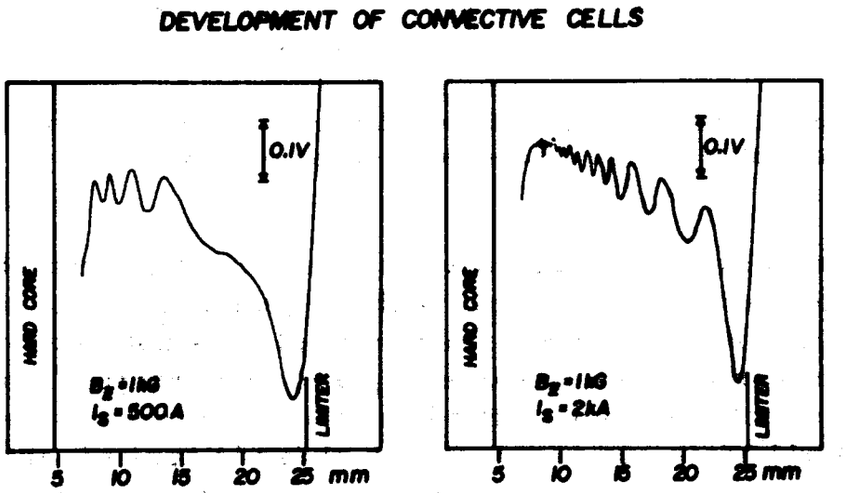

FIG. 4. Radial profiles of probe floating potential at midplane of machine in simple-ended operation. Peak density was about 10^{10} cm^{-3}.

If r_L were zero, one can show that the radial component v_r of ion drift velocity is not changed by shear, since the increase in path length is exactly cancelled by an increase in drift velocity due to the steepening of potential gradients when the spiral patterns develop. However, when the wavelength Δr of the sinusoidal potential variations in Fig. 4 becomes smaller than r_L, an ion samples different electric fields in each gyration; and its guiding center suffers a

decrease in drift velocity. We have computed the guiding-center motion for arbitrary $\Delta r/r_L$ by expanding the ion equation of motion in a sheared field in the small parameter $\epsilon \equiv r_L \partial\eta/\partial r$, where $\eta \equiv e\phi/KT = \eta_o(r) + \eta_1(r,\theta)$, η_o being the symmetric part and η_1 the asymmetric part of the potential. From Fig. 4 it is seen that $r_L\, d\eta_o/dr$ is small because η_o, though of O(1), is slowly varying; and $r_L\, \partial\eta_1/dr$ is small because $\eta_1 << 1$, though it is rapidly varying. After integrating over a Maxwellian distribution, we find

$$v_r = \frac{E_\theta}{B_z} \exp - \left[\frac{1}{4} \frac{mz}{r} \frac{r_L}{r} \frac{B_\theta}{B_z} \right]^2 \qquad (2)$$

where E_θ is the azimuthal electric field at an end plate due to an asymmetry of the form $\sin m\theta$, and the exponential factor expresses the decrease in v_r at a distance z from one end plate due to shear and finite r_L.

To compute the loss rate we assume that ions have a high probability P of being lost to the limiter or to the hard core if they reach $r = r_2$ or $r = r_1$, respectively, where r_1 and r_2 are about a Larmor diameter away from the actual boundaries; and we integrate $n v_r$ for outgoing particles over θ and z at these radii. We also assume that the equipotentials that reach r_1 and r_2 are easily populated from those that do not; a few collisions are sufficient to do this when the asymmetry is large. A typical result is shown as the "theory" curve on Fig. 2. The slope of this curve depends on the ratio of losses at r_1 to those at r_2; for the measured ratio the fit is good. The absolute magnitude of n_p depends on P and some form factors; it is also in good agreement with experiment.

We conclude that at high shear the anomalous loss can be entirely attributed to steady convection. At zero shear, convective losses are about equal to losses connected with oscillations.

3. EFFECT OF RADIAL ELECTRIC FIELDS ON DRIFT WAVES

The low-frequency oscillations in our machine are generally turbulent, with a continuous spectrum up to ~ 5 kHz. To recover the coherent oscillations of Hendel et al. [3], we have a) removed the hard core and the hole in the end plates, b) changed the collimation of K atoms to have a peak on the axis, c) increased n_p to the 10^{11} cm^{-3} range, and d) insulated the vacuum chamber and added the limiter E (Fig. 1) so that a variable potential V_c could be applied to the edge of the plasma. This oscillation amplitude vs V_c is shown in Fig. 6. With the normal bias $V_c = 0$, large turbulent fluctuations always appear. For $V_c < 0$, these fluctuations increase, and the plasma suffers "pumpout." For a range of V_c the plasma is quiescent ($n_1/n_0 < 1\%$). At a critical V_c, in this case about +2 V, coherent oscillations set in. As V_c is further increased, these oscillations change frequency, sometimes undergo a mode switch, and then become noisy. The quiescent range of V_c narrows and disappears with increasing B. The coherent waves are generally m = 1 or m = 2 modes with amplitude maximum

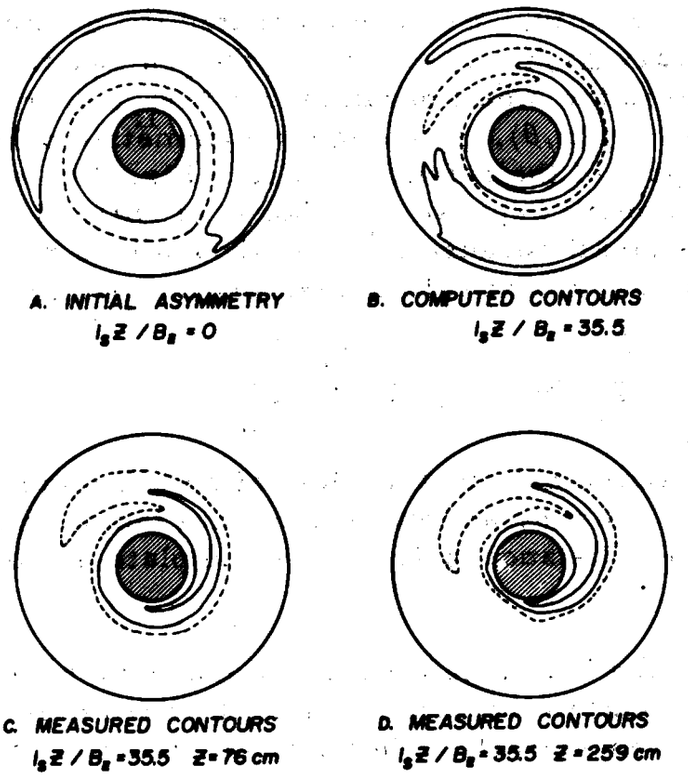

FIG. 5. Equipotential contours (A) measured with $I_s = 0$, (B) computed from (A) with a rotational transform corresponding to $I_s z/B_z = 35.5$ A-cm/G, (C) measured at $z = 76$ cm, and (D) measured at $z = 259$ cm with I_s adjusted to keep $I_s z/B_z$ constant. Some equipotentials are shown dashed for clarity. The slight difference between (C) and (D) is caused by diffusion.

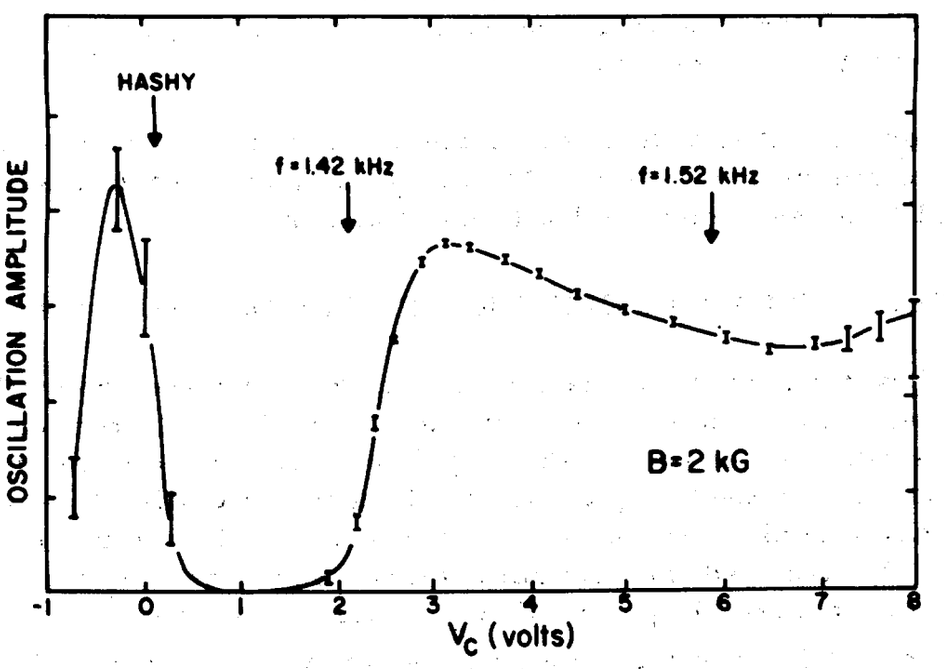

FIG. 6. Amplitude of oscillations on probe current vs vacuum chamber bias V_c. The decrease in amplitude at $V_c < 0$ is due to loss of plasma density.

at the midplane and zero at the end plates. They have an unmeasurably small $n_1 - \phi_1$ phase shift and have little effect on the plasma density. The steady-state amplitude n_1/n_0 varies from 0.01 to 0.3, depending on factors such as V_c.

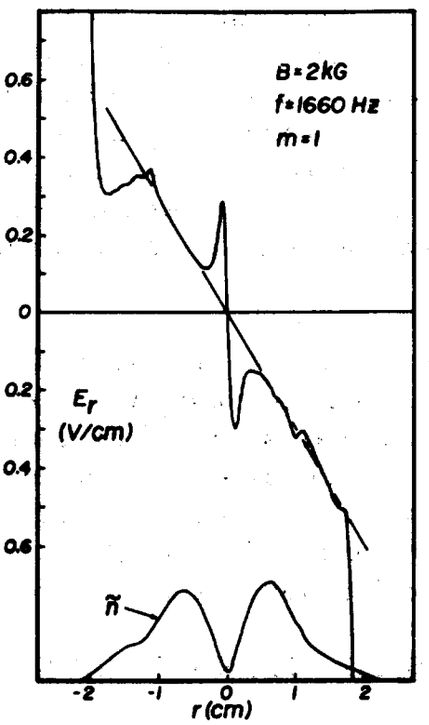

FIG. 7. Direct measurement of the radial profile of E_r in the plasma. Deviation from the solid line through the origin indicates deviation from solid-body rotation. The amplitude distribution of the oscillation is shown below.

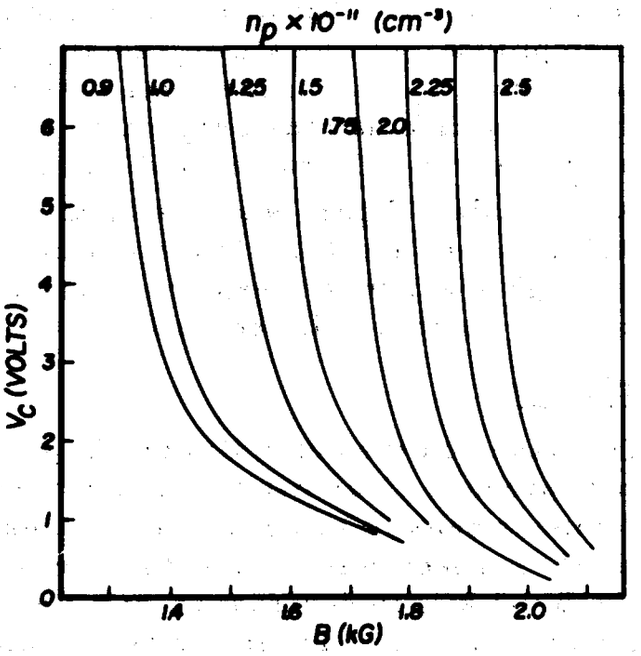

FIG. 8. Variation of the threshold value of V_c with B at various peak densities n_p. Waves can be excited by either increasing B at fixed V_c or increasing V_c at fixed B.

When V_c is varied, the radial electric field E_r in the plasma is changed from that given by Eq. (1) because of the finite ion mobility. We have measured E_r directly by a new technique employing synchronous detection of floating potential signals when the plasma is displaced by ~ 1 mm at a frequency of 17 Hz by means of auxiliary coils. Figure 7 shows an example of such a measurement. It is seen that there is a region in which $E_r \propto r$; that is, there is no velocity shear; and the

oscillation is peaked there. This appears to be a necessary requirement for coherent waves. In the case of Fig. 7, the end plates were cooler at the center than at the edge and we had $E_r > 0$; the wave velocity in the $E = 0$ frame was then $v_{De}/2$, in agreement with the results of Hendel et al. [3]. However, when $E_r < 0$ was achieved by preferentially heating the center of the end plates, there was no longer agreement with the drift-wave velocity, a result previously reported by Hartman [4].

Figure 8 shows the voltage V_c at onset of oscillations vs B for various densities. The curves approach a critical field B_c asymptotically. If $B_c/k_\perp$ is plotted against $n^{1/2}$, as done by Chu et al. [5], there is agreement with their results. The bending of the curves of Fig. 8 toward higher B at low V_c is an indication of stabilization by shear in the $\vec{E} \times \vec{B}$ drift velocity. We conclude that $E_r(r)$ has a profound effect on both the frequency and the excitation of drift waves.

4. DRIFT WAVE STABILIZATION BY MAGNETIC SHEAR

4.1. Turbulent oscillations

We have previously [2, 6] reported on the stabilization of turbulent oscillations occurring at low density ($n < 10^{10}$) with the vacuum chamber grounded. These oscillations had largest amplitudes on the inside gradient (near the hard core) but were pushed to the outside gradient, reduced in amplitude, and localized radially by the application of several kA of current I_s. Measurements with an electronic correlator showed that these fluctuations propagated at the proper velocity for drift waves in the $E = 0$ frame, and that the $n_1 - \phi_1$ phase shift was unmeasurably small. Figure 9 shows further observations indicating that the stabilizing effect of I_s is not monotonic. Reappearance of oscillations at high shear was unexpected, as was the large amount of shear needed to suppress all oscillations.

4.2 Sinusoidal oscillations

By adjusting the biases on the outer limiter E and inner limiter M (Fig. 1), we can now produce clean oscillations occurring (at $I_s = 0$) on either the outer or inner density gradient. Examples of these are shown in Figs 10 and 11, respectively. The outside waves are usually $m \approx 7$ or 8 and prefer $B \approx 3$ kG, in contrast to $m \approx 1$ or 2 and $B \approx 2$ kG for the gentler gradients of Sec. 3. These waves are line-tied at the end plates and have a single maximum near the midplane. The $n_1 - \phi_1$ phase shift is zero. In the $E = 0$ frame, the wave velocity $\omega/k_\perp$ is about $0.3\, v_{De}$; this agrees with the computed dispersion relation [7] if the finiteness of $k_\perp^2 r_L^2$ is further taken into account. Furthermore, $\omega/k_\perp$ is closer to v_{De} if V_c is close to threshold. The inside oscillations are generally $m = 1$. The wave velocity in the $E = 0$ frame is $1.5\, v_{Di}$ if the Doppler shift is computed with the value of E_r at the amplitude maximum; however, as seen on Fig. 11, E_r varies rapidly on the scale length of r_L, and the wave velocity is probably affected by the nonuniformity in E. The $n_1 - \phi_1$ phase shift is nearly 180°, with ϕ_1 slightly leading; this suggests that the inside waves are FLR-stabilized flute modes.

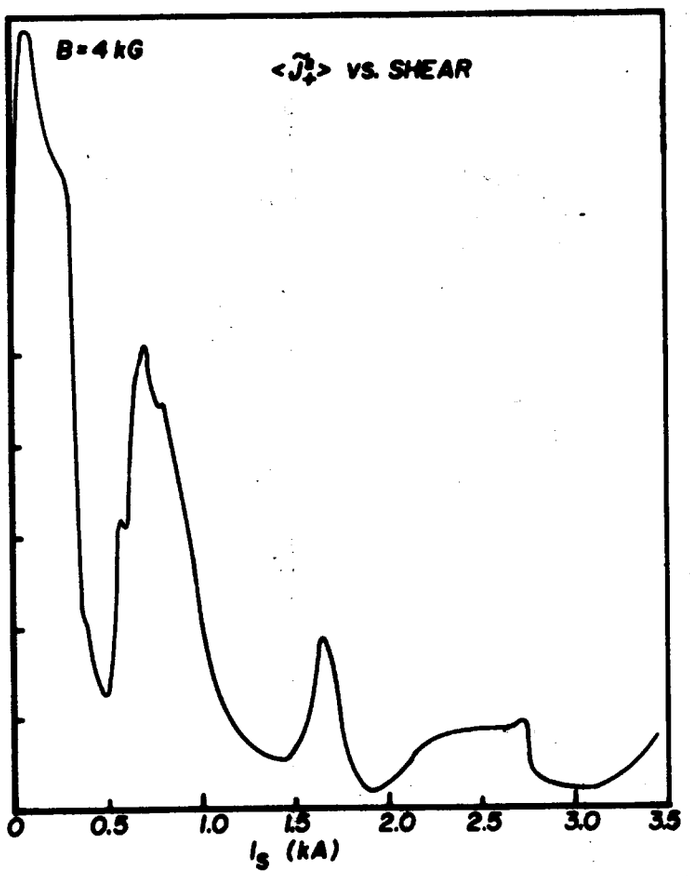

FIG. 9. Mean square oscillation amplitude at a fixed radius as a function of hard-core current.

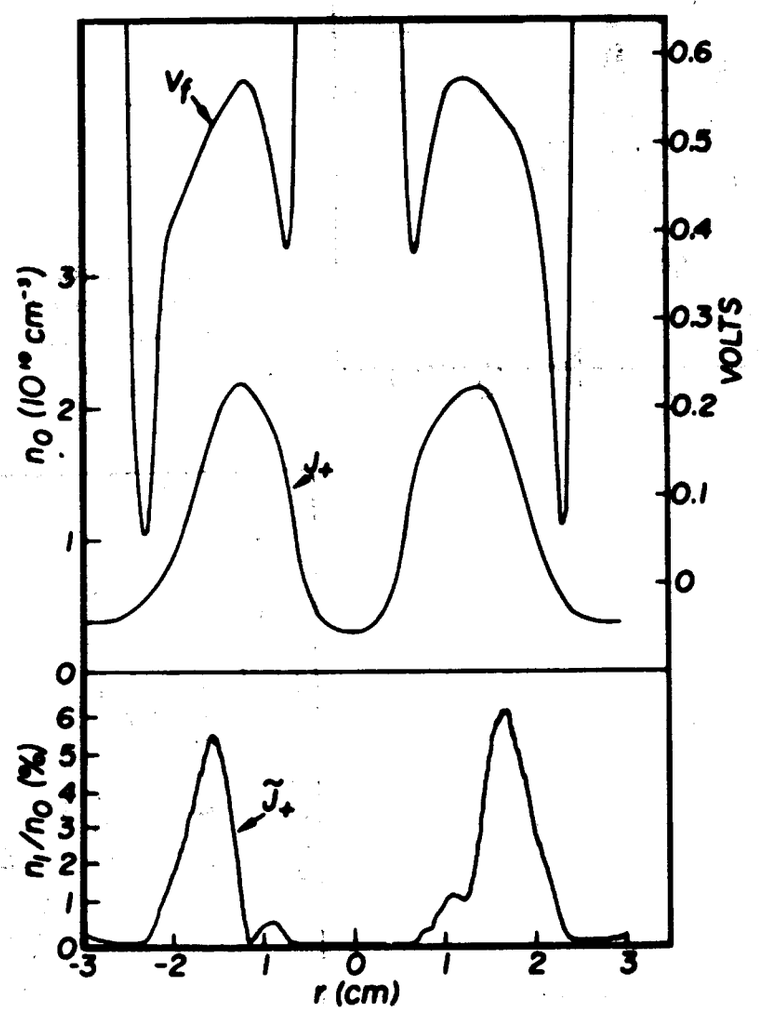

FIG. 10. Amplitude, density, and potential distributions for a 3520 Hz, m = 10 sinusoidal oscillation occurring on the outside gradient at B = 3 kG, I_s = 0.

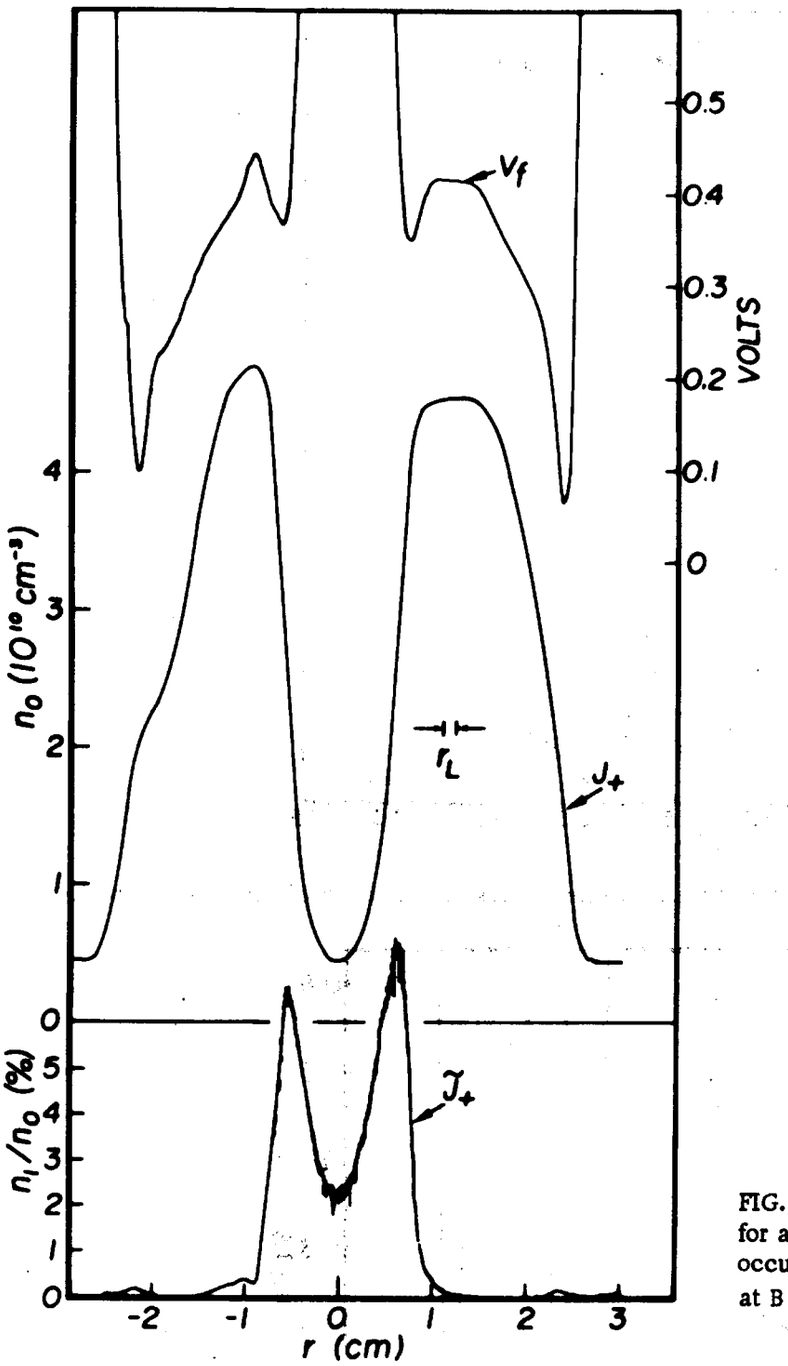

FIG. 11. Amplitude and density distributions for a 5200 Hz, m = 1 sinusoidal oscillation occurring on the inside gradient at B = 3 kG, I_s = 0.

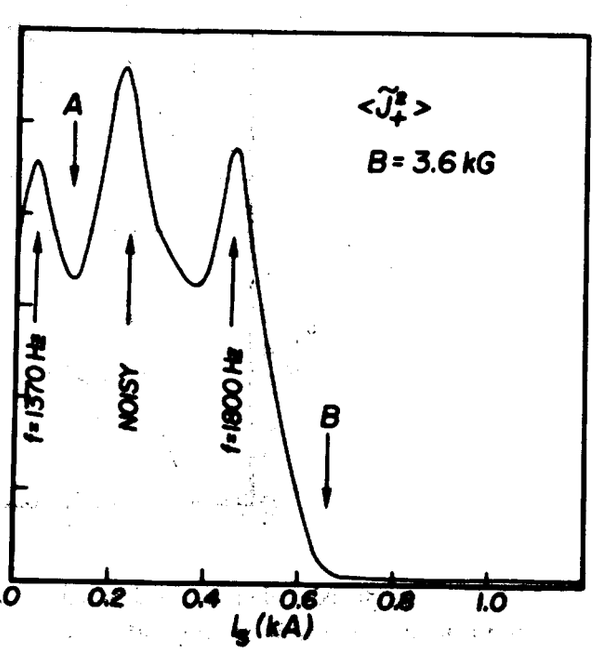

FIG. 12. Mean square oscillation amplitude vs hard-core current for coherent modes on outside density gradient.

When shear is applied to the waves on the outside gradient, the variation of oscillation amplitude with I_s is similar to that shown in Fig. 9 for turbulent waves, except that the first peak at low shear often exhibits fine structure, as shown in Fig. 12. The mode switch

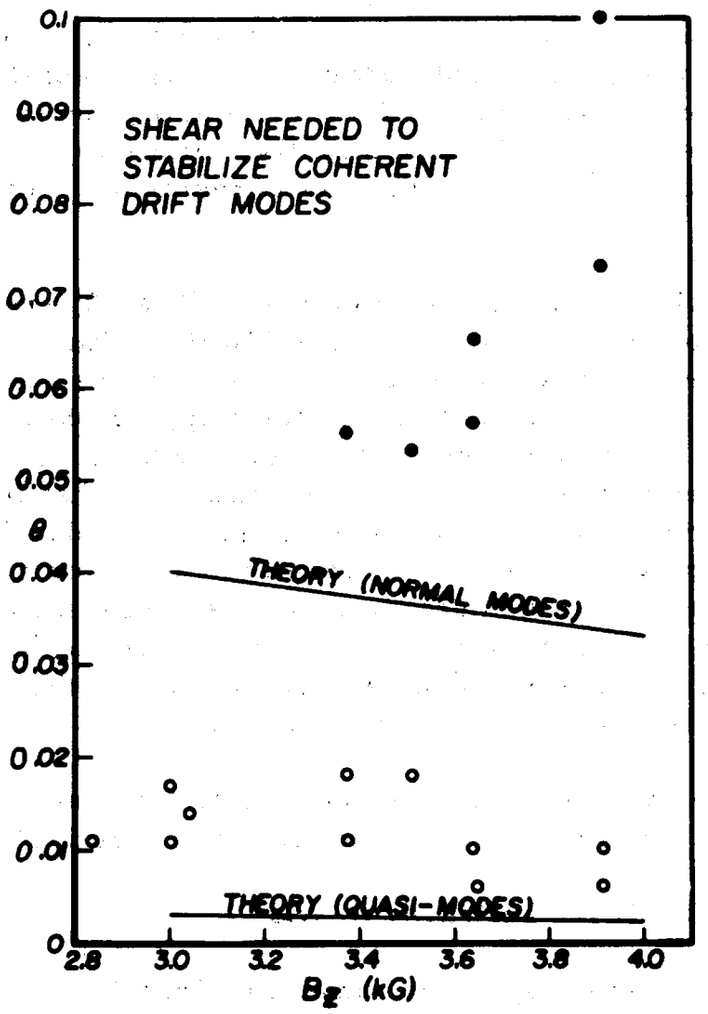

FIG. 13. Shear parameter θ required to stabilize coherent drift modes. The open points refer to point A of Fig. 12; the solid points to point B. The value of θ was taken at the radius of maximum oscillation amplitude, with r_0 defined by $n_0'/n_0 = -2r/r_0^2$. The theoretical values are computed from Krall and Rosenbluth (upper line) and Coppi et al. (lower line). For the latter we have taken the number N of e-foldings to be 3 and have used the measured value of $k_y v_D$.

at point A is probably caused by the change in E_r brought on by shear; the oscillation amplitude does not decrease greatly until point B. The shear parameters θ, defined by

$$\theta = \int_{r+r_o/2}^{r-r_o/2} \frac{\partial}{\partial r}\left[\frac{B_\theta(r)}{r B_z}\right] r\,dr$$

corresponding to points A and B are plotted in Fig. 13 for m = 7 and m = 8 modes at various B_z. Comparison is made with the two most relevant theories: that of Krall and Rosenbluth [8] for collisionless normal modes,

$$\theta_{crit} = r_L/2\,r_o \qquad (3)$$

and that of Coppi et al. [9] for resistive quasi-modes,

$$\theta_{crit} = \frac{1}{3M}\left(\frac{m}{M}\frac{\nu_{ei}}{k_y v_D}\right)^{1/2} \tag{4}$$

Since Eq. (3) predicts a higher value of θ than Eq. (4), the latter is irrelevant; at any rate, we do not observe the large radial propagation velocity expected of quasi-modes. Collisions are expected to raise the value of θ given by Eq. (3) only slightly. Since Eq. (3) is accurate only to within a factor of 2 or 3, there is agreement with the solid points on Fig. 13.

The waves which reappear at high shear (Fig. 9) are m = 1 modes with a sawtooth wave form and f ≈ 370 Hz. Their $k_{\parallel}$ is difficult to measure because of the large shear. Since the electric field pattern (Fig. 5) is so complicated, the Doppler shift is difficult to compute. In one case we found $\omega/k_{\perp} = 0.55 \pm 0.11\ v_{De}$ by averaging E_r measured at four azimuths. We calculate that the excitation of either flute or drift modes by the centrifugal force due to plasma rotation and line curvature is weaker than the excitation of ordinary resistive drift waves. We conjecture that these high-shear modes are Kelvin-Helmholtz instabilities connected with the spiral convective patterns of Sec. 2. The amplitudes are so small that these modes have no measurable effect on plasma confinement.

We conclude that our stabilization results for single modes are in agreement with theory, within the accuracy of existing theories.

5. STABILIZATION BY DAWSON RINGS

To test stabilization by short convection length, we have added internal reverse-current loops to the machine with solid end plates and no hard core, as shown in Fig. 14. As pointed out by Dawson [10], this configuration has favorable $\int d\ell/B$ everywhere. The field configuration at B_z = 2 kG, with I_D = 22.6 kA-turns in the Dawson rings, is shown in Fig. 15. In addition to minimum-$\bar{B}$ stabilization in the neighborhood of each coil, one expects viscous stabilization, since the ratio of r_L to plasma thickness d in the "bridge" region is only about 0.3.

Density profiles with the ring on and off are shown in Fig. 16. By means of obstacles inserted into the plasma (Fig. 14), we have determined that the large density near the axis with the coil on must, in the absence of oscillations, come from collisional diffusion in the bridge region. The fast diffusion there unfortunately also shortens the plasma lifetime, so that a direct comparison of oscillation levels with the coils on and off cannot be made.

Figure 17 shows the stabilization of an m = 2, f = 3.4 kHz drift wave at 2 kG. However, the corresponding density profiles (Fig. 18) show a factor of 5 decrease in density and, presumably, of plasma lifetime. The increased loss rate is due partly to collisional diffusion in the bridge region and partly to stray fields from the return leads, as

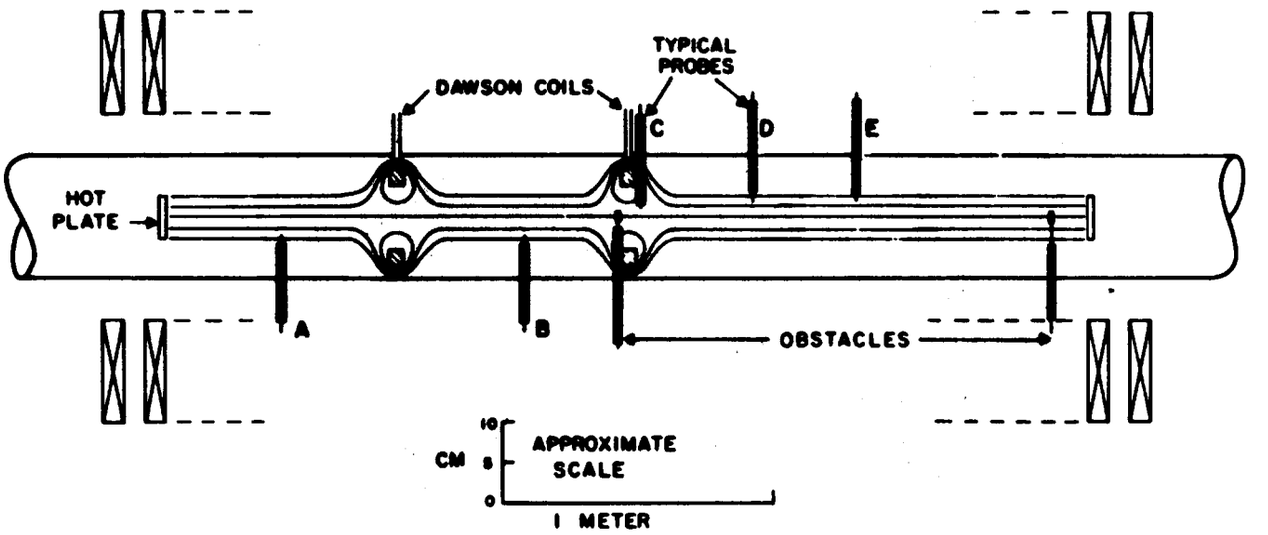

FIG. 14. Machine configuration for the Dawson ring experiment.

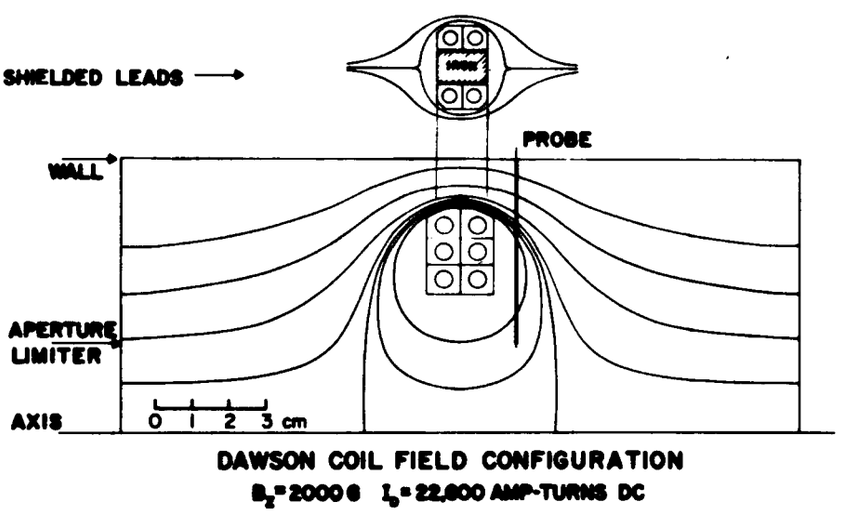

FIG. 15. Field lines around a Dawson ring in normal operation. The insert shows a top view of the computed field configuration around the leads, which are magnetically shielded with the help of an iron insert.

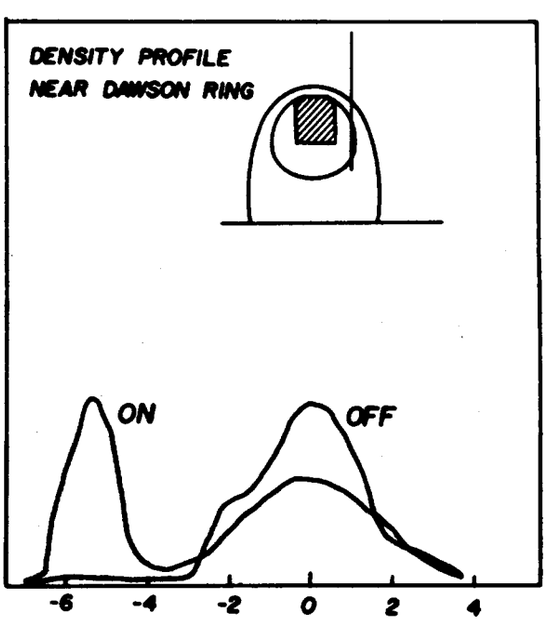

FIG. 16. Density profiles near the Dawson ring with the ring current on and off, taken with a probe in the position shown.

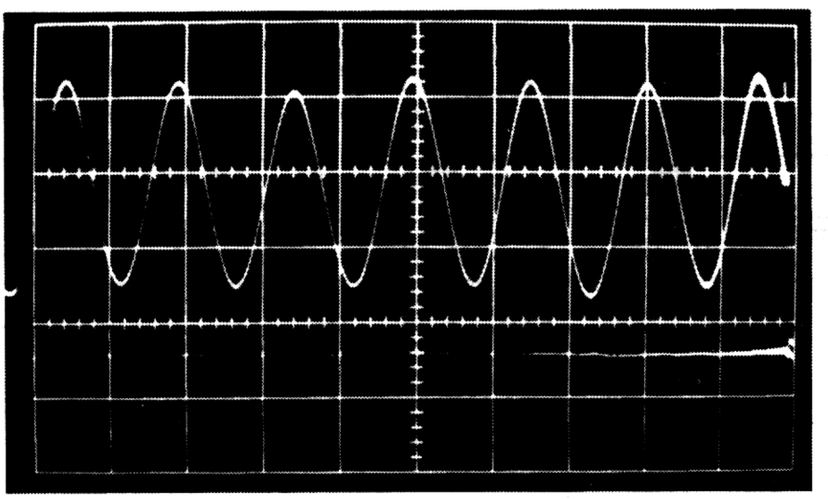

FIG. 17. Top trace: drift wave with Dawson ring off. Bottom trace: probe signal with same gain with Dawson ring on. Ac coupled; 200 μs/cm. Probe E (Fig. 14).

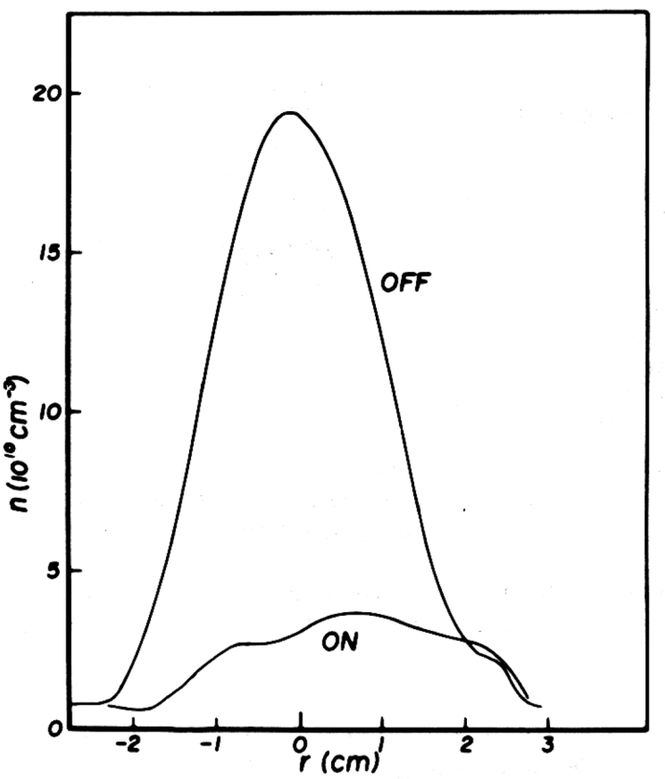

FIG. 18. Density profiles corresponding to Fig. 17. Probe D (Fig. 14).

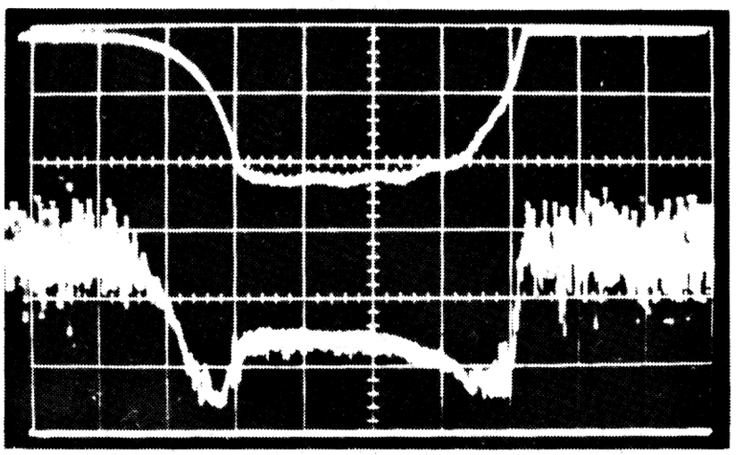

FIG. 19. Top trace: Dawson ring current, 20 kA-turns/cm, increasing downwards. Bottom trace: probe current at r = 1.5 cm, d.c.-coupled (baseline is at bottom). Sweep: 20 ms/cm, from right to left. Low density during rise and fall of current is due to the field lines intersecting the Dawson ring.

determined by reversing the sign of I_D. To reduce the diffusion loss, we increased B_z to 3.24 kG and pulsed I_D to 44 kA-turns for 0.1 sec. The oscillations were turbulent at this B_z. A typical pulse is shown in Fig. 19. Probe D (Fig. 14) was placed on the density gradient of both the "off" and "on" profiles. It is seen from the profiles of Fig. 20 that although the density decrease was only a factor of 2 , the decrease in n_1/n_0 was as much as a factor of 20. No further improvement was observed by using probe B (Fig. 14), located in a shorter section of the machine between two rings. Since a large reduction in oscillation level always accompanies the firing of the Dawson rings, we conclude that this is an efficient method for stabilizing drift waves. However, we were unable to increase the plasma lifetime.

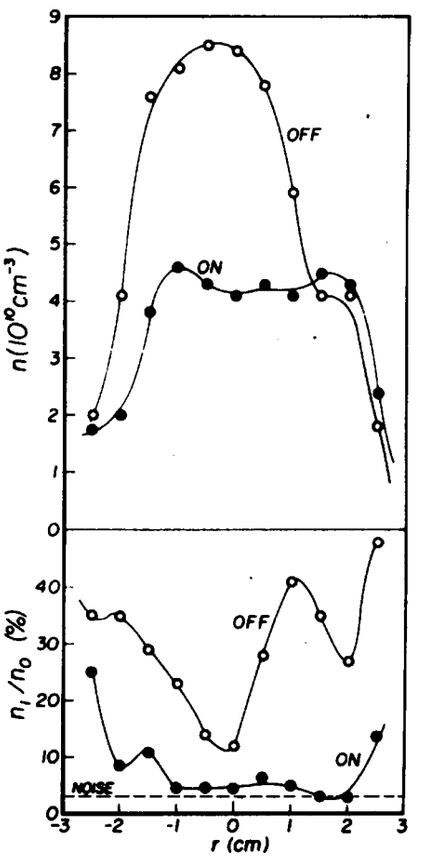

FIG. 20. Profiles of density and oscillation amplitude with B_z = 3240 G, I_D = 0, and 44 kA-turns.

REFERENCES

[1] CHEN, F. F., J. Nucl. Energy, Pt C, 7 (1965) 399.

[2] CHEN, F. F., MOSHER, D., Phys. Rev. Letters 18 (1967) 639.

[3] HENDEL, H. W., COPPI, B., PERKINS, F., POLITZER, P. A. Phys. Rev. Letters 18 (1967) 439.

[4] HARTMAN, C. W., MUNGER, R. H., Proceedings of the Conference on Physics of Quiescent Plasmas, Frascati, Italy, Pt. 1 (1967) 49.

[5] CHU, T. K., et al., Paper CN-24/E-1, this conference, Fig. 5c.

[6] CHEN, F. F., Proceedings of the Conference on Physics of Quiescent Plasmas, Frascati, Italy, Pt. 1 (1967) 145.

[7] CHEN, F. F., Phys. Fluids 10 (1967) 1647.

[8] KRALL, N. A., ROSENBLUTH, M. N., Phys. Fluids 8 (1965) 1488.

[9] COPPI, B., LAVAL, G., PELLAT, R., ROSENBLUTH, M. N., Nucl. Fusion 6 (1966) 261.

[10] DAWSON, J., private communication.